Planetary and Space Science 57 (2009) 717–724

Contents lists available at ScienceDirect

Planetary and Space Science

journal homepage: www.elsevier.com/locate/pss

The C1XS X-ray Spectrometer on Chandrayaan-1

M. Grande [a,*], B.J. Maddison [b], C.J. Howe [b], B.J. Kellett [b], P. Sreekumar [c], J. Huovelin [d], I.A. Crawford [e], C.L. Duston [f], D. Smith [g], M. Anand [h], N. Bhandari [j], A. Cook [a], V. Fernandes [l], B. Foing [o], O. Gasnaut [f], J.N. Goswami [j], A. Holland [h], K.H. Joy [b,e,i], D. Kochney [o], D. Lawrence [k], S. Maurice [f], T. Okada [n], S. Narendranath [c], C. Pieters [p], D. Rothery [h], S.S. Russell [i], A. Shrivastava [c], B. Swinyard [b], M. Wilding [a], M. Wieczorek [m]

[a] Institute of Mathematical and Physical Sciences, University of Wales, Aberystwyth SY23 3BZ, UK
[b] Rutherford Appleton Laboratory, Chilton, UK
[c] Space Astronomy & Instrumentation Division, ISRO Satellite Centre, Bangalore, India
[d] The Observatory, University of Helsinki, Finland
[e] The Joint UCL/Birkbeck Research School of Earth Sciences, Gower Street, London WC1E 6BT, UK
[f] Centre d'Etude Spatiale des Rayonnements, Université de Toulouse, CNRS, France
[g] Brunel University, UK
[h] Open University, UK
[i] Department of Mineralogy, Natural History Museum, Cromwell Road, London SW7 5BD, UK
[j] PRL, India
[k] Los Alamos National Lab, USA
[l] Berkeley Geochronology Center, Berkeley, CA, USA
[m] IPG Paris, France
[n] ISAS/JAXA, Japan
[o] ESTEC, ESA, Holland
[p] Brown University, USA

ARTICLE INFO

Article history:
Received 21 November 2008
Received in revised form
27 January 2009
Accepted 29 January 2009
Available online 20 February 2009

Keywords:
Moon
Lunar composition
X-ray spectroscopy
Chandrayaan-1
Space instrumentation

ABSTRACT

The Chandrayaan-1 X-ray Spectrometer (C1XS) is a compact X-ray spectrometer for the Indian Space Research Organisation (ISRO) Chandrayaan-1 lunar mission. It exploits heritage from the D-CIXS instrument on ESA's SMART-1 mission. As a result of detailed developments to all aspects of the design, its performance as measured in the laboratory greatly surpasses that of D-CIXS. In comparison with SMART-1, Chandrayaan-1 is a science-oriented rather than a technology mission, leading to far more favourable conditions for science measurements. C1XS is designed to measure absolute and relative abundances of major rock-forming elements (principally Mg, Al, Si, Ca and Fe) in the lunar crust with spatial resolution $\leqslant$25 FWHM km, and to achieve relative elemental abundances of better than 10%.

© 2009 Elsevier Ltd. All rights reserved.

1. Introduction

The Chandrayaan-1 X-ray Spectrometer (C1XS) is a compact X-ray spectrometer for the Indian Space Research Organisation (ISRO) Chandrayaan-1 lunar mission, which was successfully launched on 22 October 2008. It exploits heritage from the D-CIXS instrument (Grande, 2001; Grande et al., 2003, 2007; Swinyard et al., forthcoming) on ESA's SMART-1 mission (Racca et al., 2002). However, by comparison with SMART-1, Chandrayaan-1 is a science-oriented rather than a technology mission, leading to far more favourable conditions for science measurements. C1XS is designed to measure absolute and relative abundances of major rock-forming elements (principally Mg, Al, Si, Ca, Ti and Fe) in the lunar crust with spatial resolution ~25 km.

The C1XS hardware was designed and built by an international team led from the Rutherford Appleton Laboratory (RAL), STFC. The Principal Investigator is Prof. M. Grande at Aberystwyth University. There is also a major science and design contribution from ISRO Satellite Centre, Bangalore, India; CESR, Toulouse, France provides 3-D Plus video processor integrated circuits, and there is an important contribution to the detector characterisation from Brunel University. The Science team is chaired by Dr. I.A. Crawford of Birkbeck College, London. In order to record the incident solar X-ray flux at the Moon, C1XS carries an X-ray Solar

* Corresponding author.
E-mail address: M.Grande@aber.ac.uk (M. Grande).

0032-0633/$ - see front matter © 2009 Elsevier Ltd. All rights reserved.
doi:10.1016/j.pss.2009.01.016

Monitor (XSM) provided by the University of Helsinki Observatory, Finland. C1XS is primarily funded by ESA with partial support to RAL from ISRO.

D-CIXS was able to demonstrate an ability to sense remotely elements in the top few micrometers of the lunar regolith, in particular Mg, Al, Si, Ca and Fe (Grande et al., 2007; Swinyard et al., forthcoming). The Ca detections represented the first unambiguous remote sensing of calcium. More recent detailed analysis shows that in favourable conditions titanium is also observed (Swinyard et al., forthcoming). Other companion papers describe in more detail the science goals (Crawford et al., 2009), the instrument construction (Howe et al., forthcoming) and the calibration status (Kellett et al., 2009).

2. Instrument requirements

Solar irradiation excites fluorescent emission from the lunar surface; by measuring this emission, whilst at the same time monitoring the incident solar X-ray emission, we are able to map the absolute elemental abundances of the main rock-forming elements on the Moon. In addition, during bright flares, we detect localised concentration levels of key minor elements. The timing of the Chandrayaan-1 mission, ensuring that the spacecraft arrives at the beginning of the rising phase of the solar activity cycle, with near Solar maximum flux levels expected at the end of its nominal mission, is well suited for this purpose. The 10× higher solar X-ray fluxes, combined with the excellent (85–115 km near

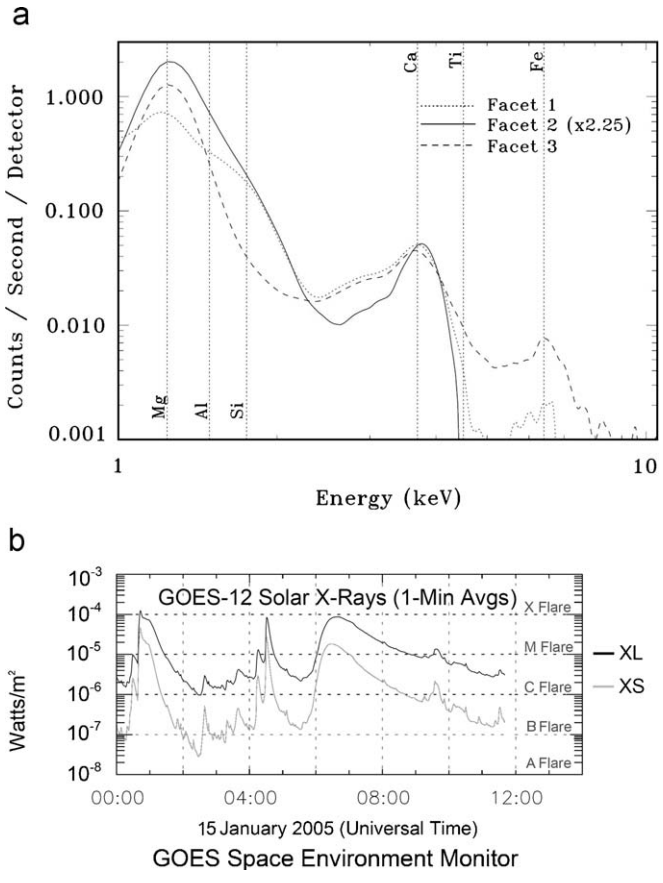

Fig. 1. (a) Fluorescence spectra obtained by D-CIXS on SMART-1 on 15 January 2005, indicating an ability to remote sense elements in the top few micrometers of the Lunar regolith, in particular Mg, Al, Si, Ca and Fe, as indicated by vertical lines (Grande et al., 2007). Vertical lines indicate the expected position of these elements. (b) Also shown is the 10 Å (black) and 1 Å (grey) (TBC) Solar X-ray illumination at the time, derived from GOES Space Environment Monitor data, indicating the high variability of the Sun as an X-ray source. Times are indicated on the *x*-axis in hours. Note the conventional A,B,C,M,X nomenclature for flare levels are indicated on the left-hand side of the plot.

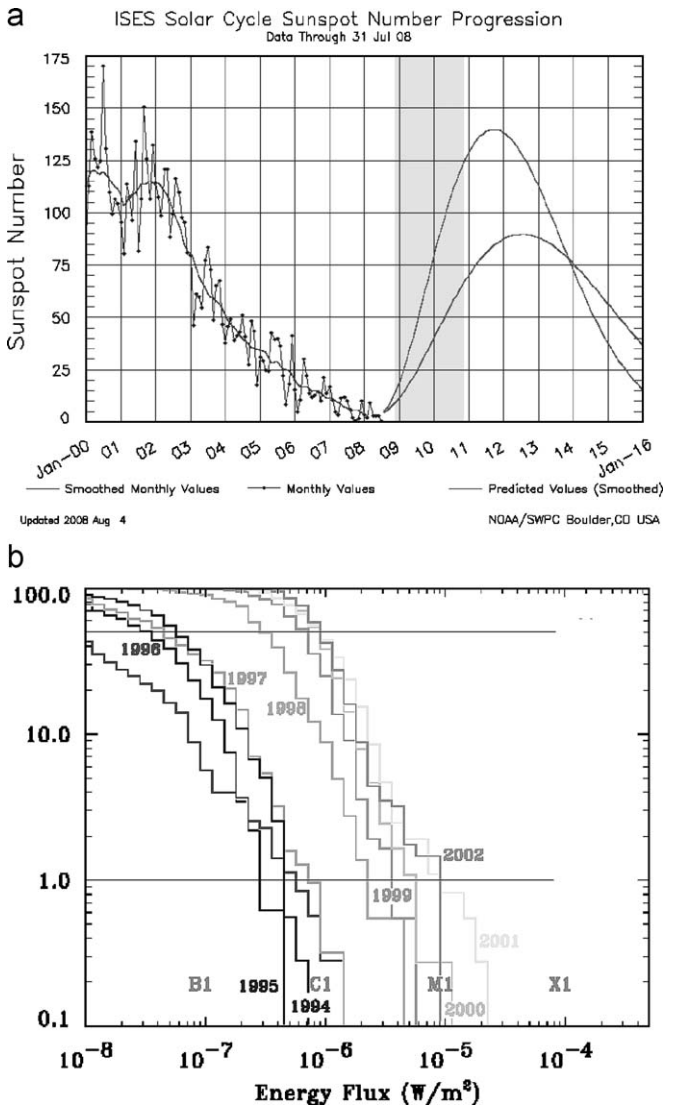

Fig. 2. (a) Past blue and predicted red solar cycle variation (NOAASpace Weather Prediction Center) during the Chandrayaan-1 missions (Ref.). Note that whilst SMART-1 took place during a decline into solar minimum, Chandrayaan-1 will be launched in the ascending phase of the cycle (shown by shaded region), which is predicted to be close to peak by the end of the mission. The two red lines indicate alternative predictions. (b) Cumulative distribution of 1 min solar flare date from the previous cycle, indicating probability of illumination above a certain illumination level more. To obtain predicted fluxes add 11 to the year.

Table 1
Energies (eV) of relevant X-ray fluorescent lines. [See discussion for those lines detectable by C1XS.]

Element	$K\alpha_1$	$L\alpha_1$
Oxygen	524.9	–
Sodium	1040.98	–
Magnesium	1253.60	–
Aluminium	1486.70	–
Silicon	1739.98	–
Potassium	3313.8	–
Calcium	3691.68	–
Titanium	4510.84	–
Iron	6403.84	705.0

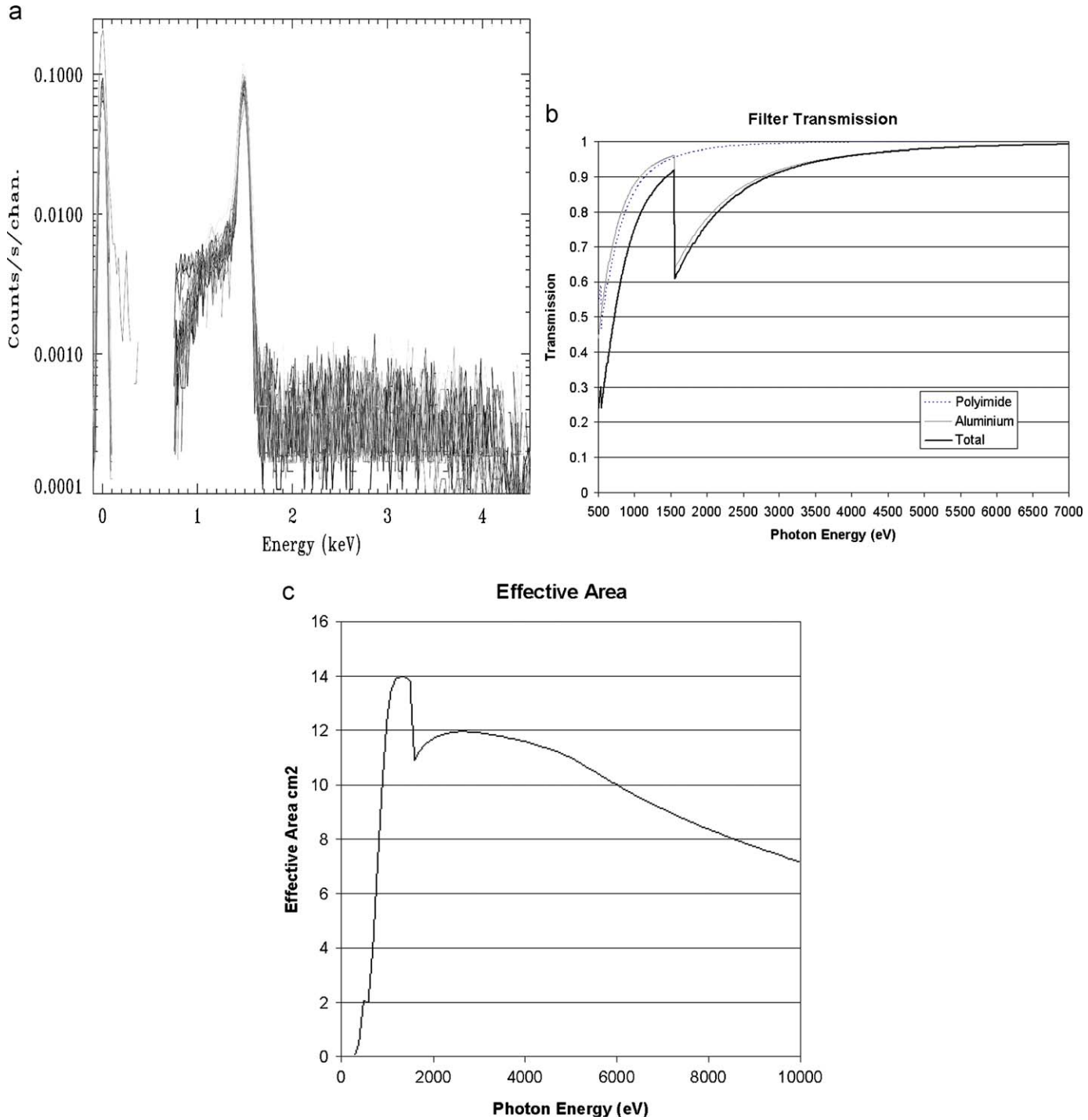

Fig. 3. (a) Measured performance at low energies in C1XS illustrating the reponse of all 24 SCDs to Al Kα (1.487 keV) and the low-energy cutoff of the instrument at 750 eV, derived during calibration (Kellett et al., 2009). Note the excellent alignment and uniformity of the 24 different responses. (b) Calculated filter transmission for 800 nm of Al-coated polyimide over the active range of the instrument. (c) Calculated effective area of the instrument, plotted against energy, based on geometry, and filter and detector specification, but neglecting electronic losses. Note the rapid loss of effective area below 1 keV.

circular) orbit, will help ensure that C1XS can carry out enormously enhanced science compared to SMART-1.

The nominal mission duration is 2 years. Given the Moon's 28 day rotation, this corresponds to 25 daylight overflights for each 25 km FWHM field-of-view (FOV) on the surface, and 16 within 60° of zenith illumination. Illumination conditions will be different for each overflight, both for geometrical reasons, but much more importantly because of the huge variations in the solar X-ray illumination that takes place on timescale of minutes, as shown in Fig. 1b. At solar maximum, expected at or shortly after the end of the Chandrayaan-1 mission, X-ray illumination is above C1 category flare conditions for ~40% of the time (see Fig. 2), based upon statistics from the previous cycle. In a 2-year solar maximum mission, each pixel would be sampled with near zenith C1 illumination on average 6 times. A more precise calculation shows around 95% probability of a pixel being illuminated at greater than C1 at some point during the mission, which is sufficient to return the required spectral resolution. Around 10% of

pixels should be illuminated with greater than M1 at some point during the mission. We note that C1XS is to be launched at around the beginning of solar cycle, and that fluxes are therefore very sensitive to variations of a few months in the upturn in the solar cycle relative to the launch date. Fig. 2 is based on the current (27 June 2008) best NOAA SEC predictions (Biesecker, 2008) showing the high and low predictions. Currently (Keating, 2008) the cycle appears to be an average 11-year cycle. However, flare numbers are very low compared to recent cycles. A 6-month mission extension, at full Solar maximum, would certainly yield large increase in the quality of X-ray illumination.

We can investigate minor elements like sodium, phosphorous and sulphur, which provide great insight into lunar evolution. The energy range of CIXS is 0.8–7 keV, and the energy resolution at launch is ~160 eV FWHM at 8 keV (2%), sufficient to resolve all the main fluorescence lines of interest, as shown in Table 1. The ability to detect sodium (Kα at 1.043 keV) if it is present in significant quantities is particularly interesting. It may also be possible to detect the iron L-lines, which will enable C1XS to observe iron in all illumination conditions. For these reasons, particular care has been taken in defining the lower energy cutoff, as illustrated in Fig. 3a. The low-energy discriminator level is software commandable, but whilst in theory it could be lowered to include the oxygen Kα line at 525 keV, and the detectors have some sensitivity at these low energies, the filter cutoff shown in Fig. 3b would preclude useful information. Since the oxygen concentration across the highly oxidised lunar surface does not vary outside a range 41–46% (e.g., Lawrence et al., 1998), these data would not in any case yield significant new information. However, at the start of mission, we will have sufficient sensitivity for the Fe Lα line at 705 eV, which greatly improves the functionality of the instrument, enabling Fe concentrations to be measured in all illumination conditions. Fig. 3c shows the calculated overall effective area of the instrument, excluding electronic considerations.

In order to obtain good absolute elemental abundances by the X-ray fluorescence technique, it is essential to continuously monitor the solar X-ray flux, which excites the lunar emission. To this end the CIXS instrument includes an X-ray Solar Monitor, designed and delivered by the University of Finland. The XSM will also provide a scientific bonus in providing a long time series of the solar X-ray spectra with high spectral resolution and full energy band coverage.

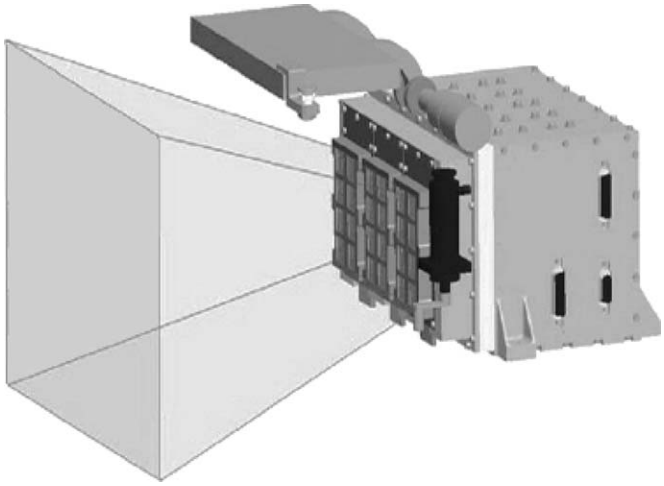

Fig. 4. CAD image of the C1XS instrument showing coalligned front detectors, deployable radiation shield and 14O field-of-view. Note light-coloured thermal gasket separating cool detector enclosure from electronics case to the right. The instrument design aims to keep detector temperatures below −17.5 °C, which ensures optimum signal-to-noise and stability, as well as improving radiation tolerance. The table below gives a summary of the instrument parameters for C1XS and XSM.

C1XS	
Mass	5.5 kg
Volume (with door closed)	250 mm wide, 150 mm tall, 190 mm deep
Power	6.3 W (Standby)
25.5 W (operating)	
Energy range	0.8–20 keV
Geometrical detector area	24 cm^2
Field-of-view	14° (FWHM)
28° (full angle)	
Supply voltage	20 to 45 V
Temperature range	
Electronics	−50 to +80 (off)
	−20 to +40 (operating)
Detector module	−50 to +80 (off)
−40 to +0 (operating)	
Readout frequency	87,381 kHz
Data volume (average)	36 Mbits/orbit
XSM	
Nominal energy range	1.2–20.0 keV
Energy resolution	200 eV at 5.9 keV
Number of spectral channels	512
FOV(circular) diameter	104°
On-axis geometric area	0:001 cm^2

3. Instrument

The baseline instrument design (see Fig. 4) consists of 24 nadir pointing Swept Charge Device (SCD) detectors (Howe et al., forthcoming). A traditional box collimator defines the field-of-view of each SCD, resulting in a triangular angular sensitivity with 50% of the X-ray signal deriving from 14° of the collimator aperture, corresponding to 25 km on the lunar surface from Chandrayaan-1's circular 100 km orbit. Due to the highly elliptical orbit of SMART-1, the corresponding values for D-CIXS ranged from 32 to 315 km. The uniform spatial resolution of C1XS will greatly simplify the data analysis. The C1XS collimator stack differs from that on D-CIXS in that it is machined numerically, as opposed to by lithographic construction (Grande et al., 2003; Howe et al., forthcoming). Fig. 5 shows the flight instrument during calibration.

A deployable door protects the instrument during launch and cruise, and also provides a ^{55}Fe calibration X-ray source for each of

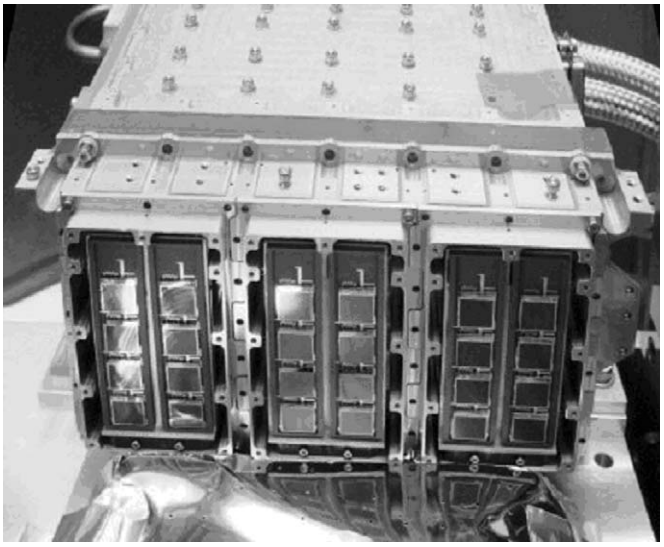

Fig. 5. View of the C1XS flight instrument during calibration. The collimator assembly and doors have not yet been added, so that the 24 swept charge detectors, arranged in ladders of four, are clearly seen.

the detectors, allowing in flight calibration to be performed. The source strength is sufficient over the 2-year mission for gain calibration to the required 1% accuracy to be obtained within 10 min. This will also allow energy and FWHM calibrations of sufficient accuracy to be obtained.

4. Detectors

The Swept Charge Device detectors (Gow et al., 2007) provide high detection efficiency in the 0.8–7 keV range, which contains the X-ray fluorescence lines of interest. The SCD is a CCD-like device which achieves near Fano-limited spectroscopy below −10 °C. It has a continuous one-dimensional readout architecture, which is otherwise similar to a conventional CCD, and a 1.1 cm^2 detector area. The instrument design aims to keep detector temperatures below −17.5 °C, which provides sufficiently low SCD leakage current to ensure optimum signal to noise and stability, as well as improving radiation tolerance.

The detectors are shielded from the lunar UV and visible albedo, as well as protons below 180 keV and low energy electrons, by two layers of 400 nm aluminized polyimide filtering (Fig. 3b shows their calculated X-ray transmission). Careful thought has been given to the radiation shielding, in what is already a comparatively low radiation environment orbit. It will now consist of a 4-mm-thick aluminium electronics box with 3 mm of copper and 6 mm of tantalum behind the SCD modules. Due to the low altitude, the spacecraft is well-shielded from the front by the Moon itself. The collimator structure and additional tantalum provide additional shielding for oblique angles.

The principal instrument requirement is a spectral resolution sufficient to clearly resolve the three common light rock-forming elements (Mg, Al, Si). As will be seen from Table 1, this implies an energy resolution better than 250 eV at 1–2 keV. Fig. 6a and b indicates that in laboratory calibration this condition is comfortably met. The effects of radiation tests on SCD detectors from the same batch are shown in Fig. 7 suggesting that even at the end of life, the performance requirements will be met. There is some uncertainty in the predicted range of exposures due to the sensitivity to the phase of the solar cycle. The figures shown reflect the fact that as of present, large solar flares have not been observed in the current rising cycle. Note by comparison the reduced energy resolution of D-CIXS after the heavy radiation doses it incurred during its extended cruise phase to the Moon (Grande et al., 2007).

The maximum expected count rate for the C1XS instrument will be 2000 counts per second for all 24 detectors, for an X20 flare, acceptable within the instrument limit of 5500 cps (see Howe et al., forthcoming). Additional refinements to the electronics, onboard software and thermal design will also greatly increase detector stability and signal-to-noise ratio over what was achieved on D-CIXS [Grande et al., 2007]. Electronic noise has been reduced to 60 eV. A detailed account of the technical development is given in Howe et al. (forthcoming).

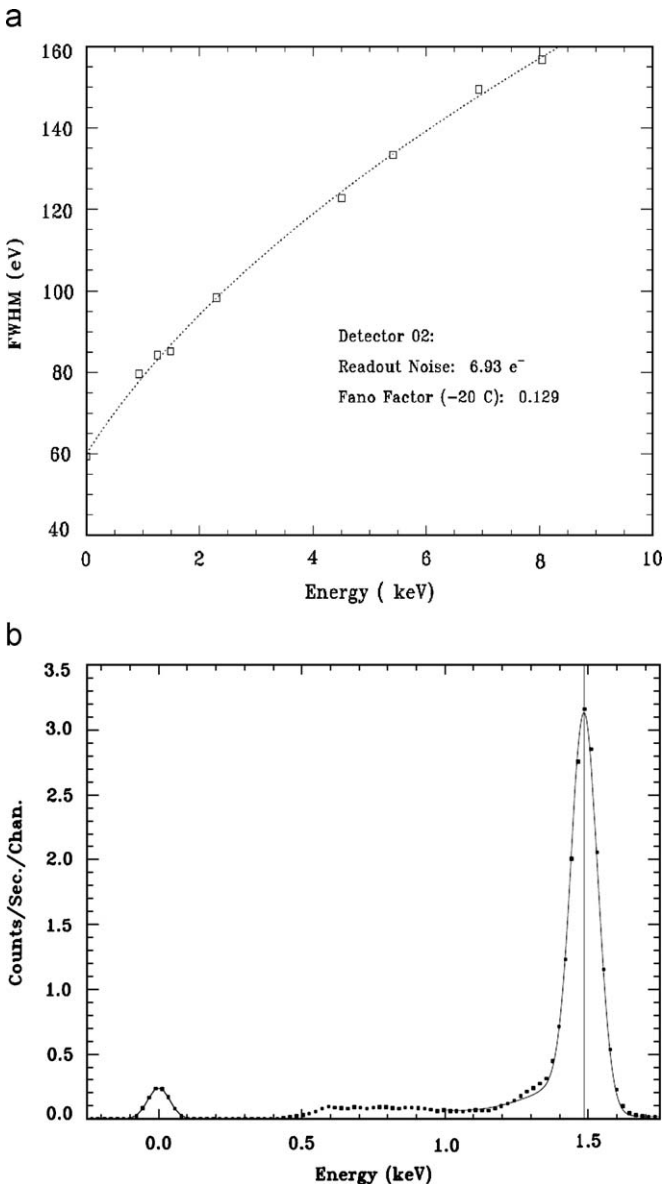

Fig. 6. laboratory performance of C1XS as obtained during calibration (Kellett et al., 2009). (a) Measured combined FWHM of the detectors and readout electronics as a function of energy. (b) Example showing measured resolution at the 1.49 keV aluminium $K\alpha_1$ line and also the well-separated zero energy electronic noise peak. Note the major improvement over the performance of D-CIXS as shown in Fig. 1.

5. X-ray solar monitor

The X-ray solar monitor is based on the SMART-1 XSM (Huovelin et al., 2002) and consists of a separate silicon detector unit on the spacecraft. The non-imaging HPSi PIN sensor has a

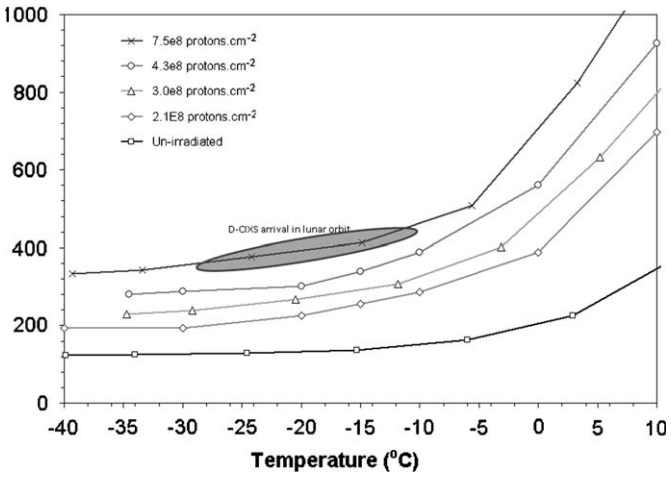

Fig. 7. Swept charge device energy resolution shown as FWHM at the Mn-Kα line vs. temperature, before and after radiation testing. The specified maximum operating temperature is −17.5 °C. Note the favourable comparison with D-CIXS FWHM shown in between the dashed lines.

wide field-of-view to enable Sun visibility during a significant fraction of the mission lifetime, which is essential for obtaining calibration spectra for the X-ray fluorescence measurements by the C1XS spectrometer. The energy range (1–20 keV), spectral resolution (about 200 eV at 6 keV) and sensitivity (about 7000 cps at a flux level of 10^{-4} W m^{-2} in the range 1–8 keV) are tuned to provide optimal knowledge about the solar X-ray flux, matching well with the activating energy range for the fluorescence measured by C1XS.

As has been remarked, the X-ray flux rises rapidly during a major solar flare. However, this is frequently followed by an increase in the penetrating background radiation, at a time-delay dependent on the energy and the geometry of the interplanetary magnetic flux. Thus, it is still in general possible to use the brightest X-class events for fluorescence spectroscopy, and the very high fluorescence count rates obtained will be invaluable in revealing the concentrations of minor elements in the regolith. Typical time delays are of up to 1 h duration.

6. Predicted response

The baseline specification is to achieve 10% relative elemental abundance accuracy from a single overflight of a 25 km pixel in C1 solar flare conditions, and we consider the instrument response in terms of this baseline situation. Fig. 8 shows the calculated response to fluorescence from a representative Lunar basalt, using our physical instrument model, indicating the minimum detectable flux for C1 flare with a 14° opening angle for a real detector area of 24 cm^2 detector and a 0.8 throughput collimator expressed as counts/s/keV and a 100 eV resolution. The calculation includes calibration and electronic efficiency data from D-CIXS. The smooth line is the 3 sigma detection limit for a 16 s integration, typical for overflight of a single pixel. It is seen that the Mg, Al and Si lines are well-resolved for this baseline illumination condition. As an example of inferred performance under flare conditions, Fig. 9 shows a comparison of predicted C1XS response in quiet and flare conditions to an actual event observed by D-CIXS, described in the accompanying paper by Swinyard et al. (forthcoming). Note the greatly increased signal for the low-energy Mg, Al and Si lines, and the excellent signal-to-noise ratio in the Ca, Ti and Fe lines at the peak of the flare. Again, instrument response (100 eV) is derived from C1XS laboratory calibrations (Kellett et al., 2009).

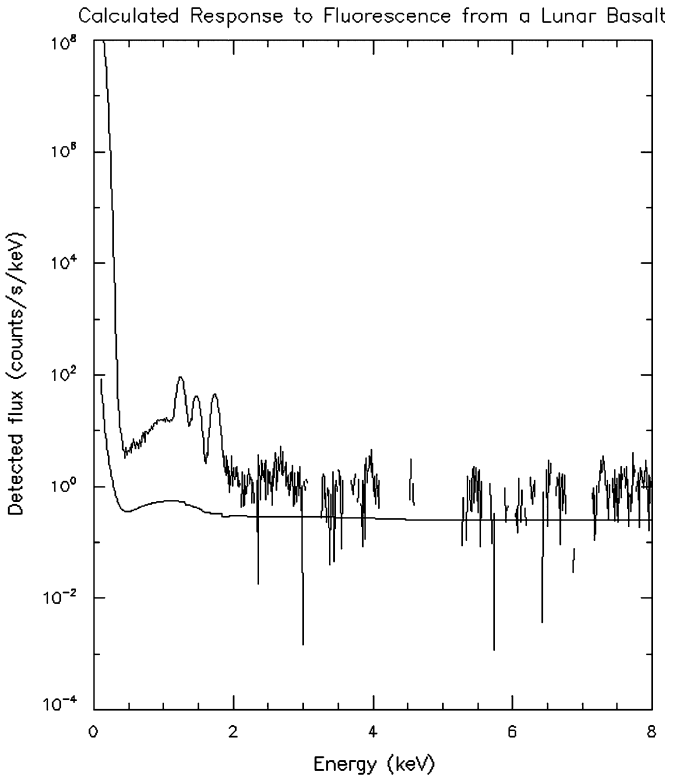

Fig. 8. Calculated response to fluorescence from a representative Lunar basalt, using our physical instrument model, indicating the minimum detectable flux for C1 flare with a 14° opening angle for a real detector area of 24 cm^2 detector and a 0.8 throughput collimator expressed as counts/s/keV and 100 eV resolution. The calculation includes calibration and electronic efficiency data from D-CIXS. The smooth line is the 3 sigma detection limit for a 16 s integration, typical for overflight of a single pixel. It is seen that the Mg, Al and Si lines are well-resolved in this baseline illumination condition.

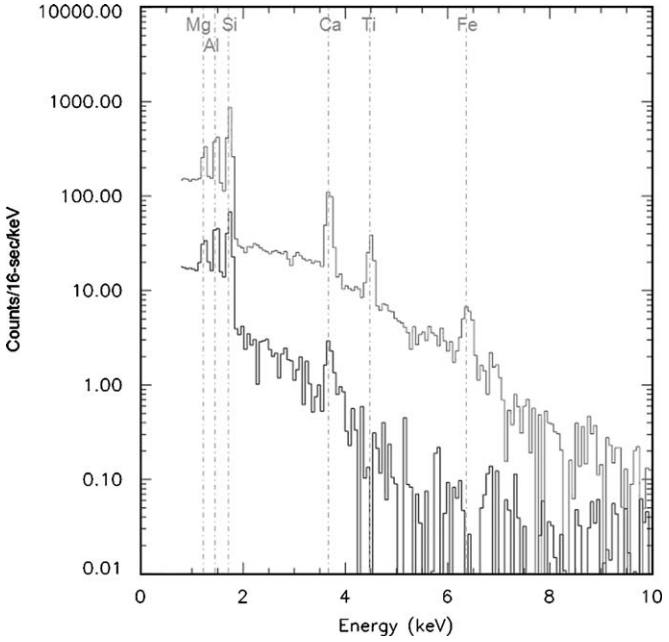

Fig. 9. Simulated C1XS spectrum for the November 18 flare based on individual 16 s integrations. The lower line (black) shows the spectrum detected during the quiet period just before flare begins, while the upper line (grey) shows the spectrum obtained at the peak of the flare.

Accurate knowledge of the input solar spectrum is essential for determination of elemental abundances. A linear difference in solar input will leave the relative line ratios unchanged. However, this is not the case if the shape of the input solar spectrum changes. Fig. 10 shows 4 different flare levels (A5, B1, C1, M1), with the output spectra that would result. We note that the apparent line ratios are very significantly modified. The point is made even more clear in Fig. 11, which shows three different models of C1 solar flares (Mewe et al., 1985; Clark and Trombka, 1997). The calculated lunar fluorescent spectra, which would be detected following scintillation of lunar basalt, are also shown. In this case the predicted line ratios are modified by more than $\pm$10%.

This emphasizes the vital importance of accurate monitoring of the solar input spectrum, as well as good codes to forward model the expected lunar X-ray fluorescence for different possible regolith compositions. Thus, whilst elemental abundance ratios may be useful diagnostics in our initial analysis, final estimations of lunar elemental abundance ratios will require detailed modelling (see Swinyard et al., forthcoming). One of the lessons learned from D-CIXS was the critical importance of fully characterizing the input solar spectrum, if one is to derive absolute lunar elemental surface abundances. In comparison to D-CIXS, C1XS and XSM are far better calibrated. Details of the results obtained in the calibration campaign of the C1XS instrument are given by Kellett et al. (2009).

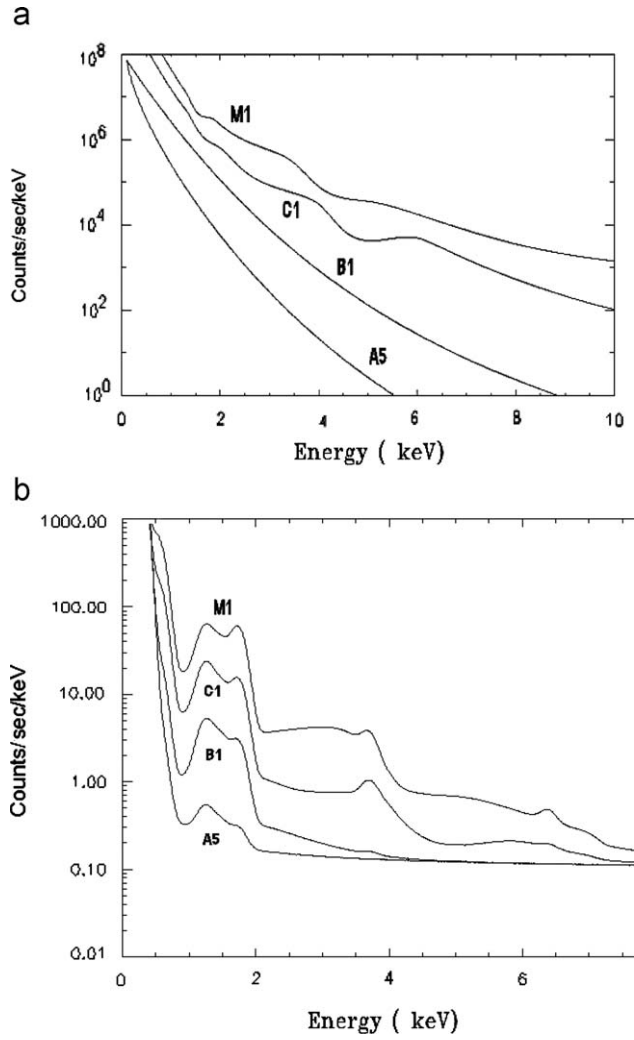

Fig. 10. Calculated lunar fluorescent spectra, which would result from four different solar flare input levels (A5, B1, C1, M1). Upper panel (a) shows input flare spectra while lower panel, (b) shows the calculated detected flux from a lunar basalt, in counts/s/kev, as detected by C1XS. Note that calcium and iron lines (at 3.7 and 6.4 keV) are only seen for the harder input spectra of the stronger flares.

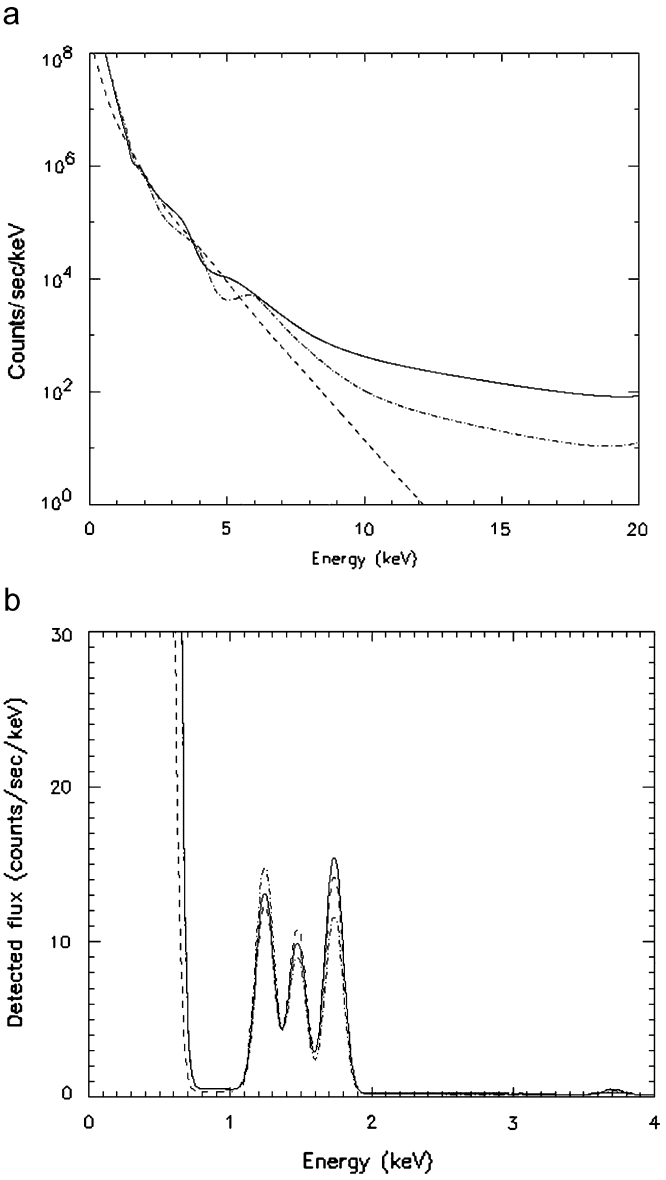

Fig. 11. (a) Three different models of C1 solar flares (dashed line, Mewe et al. (1985); dash-dotted line, Clark and Trombka (1997); full line, M1 flare from Clark and Trombka, (1997) normalised to C1 intensity). (b) Resulting calculated lunar fluorescent spectra, as detected by C1XS, that would result. Note the complete reversal of the line ratios which would be observed.

7. Science goals

A detailed description of the science objectives for the instrument and the match of its capabilities to key questions is given in a companion paper by Crawford et al.

C1XS will arrive at the Moon in the run up to the maximum of the solar cycle, and the high incident X-ray flux observed from an orbit optimised for science, and coupled with good instrumental energy resolution, means that we will obtain composition data accurate to better than 10% of major elemental abundances over the entire surface. We note that observations of major element abundances for regions where samples have been obtained by the Apollo and Luna missions will be used to validate the calibration of C1XS measurements. Thus, C1XS will be well-placed to make significant contributions to lunar science in a number of areas.

Specifically, C1XS will determine the major element geochemistry (and especially Mg/Si and/or Mg/Fe elemental ratios) in the main lunar terrain types (i.e. Procellarum KREEP Terrane, South Pole-Aitken Basin, and the Farside Highlands; Jolliff et al., 2000) and establish the geographical distribution of the magnesian suite of rocks. A key ambition is to determine the large-scale stratigraphy of lower crust (and possibly crust/mantle boundary region) by measuring the elemental abundances of the floor material of large basins not obscured by mare basalts (e.g., SPA and other farside basins), and the central rings and ejecta of large basins, which expose material derived from depths of many tens of km. In addition, determination of the crustal aluminium abundance and distribution is important for the assessment of lunar refractory element enrichment, and C1XS-derived aluminium abundance maps will thus constrain models of lunar origins. Last but not the least, the ~25 km spatial resolution will enable C1XS to address a number of smaller-scale geological issues (e.g., the composition of discrete mare basalt lava flows and, pyroclastic deposits), which also refine our understanding of lunar geological evolution (Joy et al., 2008; Crawford et al., 2009).

8. Conclusions

The C1XS instrument is optimised to perform X-ray spectroscopy in the framework provided by the ISRO Chandrayaan-1

mission to the Moon. This is highly suitable for producing high-quality data on lunar composition derived from Lunar X-ray fluorescence spectra, taken in the approach to Solar maximum. The instrument represents a considerable refinement on the original D-CIXS instrument on SMART-1. It is expected to provide data of the spatial and the spectral resolution required to produce significant progress in lunar science.

Acknowledgements

The C1XS instrument development was supported with funding from ESA Science and Technology Research Programmes. Major thanks for support are due to RAL/STFC, and also ISRO ISAC. Additional hardware was provided by CESR, Toulouse and University of Helsinki Observatory. J. Carter of Aberystwyth University is thanked for recalculating Fig. 8.

References

Biesecker, D., the NOAA/SEC Solar Cycle 24 Panel. The Solar Cycle 24 Consensus Prediction; Web document 〈www.swpc.noaa.gov/SolarCycle/SC24/Biesecker.ppt〉, June 2008.

Clark, P.E., Trombka, J.I., 1997. Journal of Geophysical Research 102, 16631.

Crawford, I.A., Joy, K.H., Kellett, B.J., Grande, M., Anand, M., Bhandari, N., Cook, A.C., d'Uston, L., Fernandes, V.A., Gasnault, O., Goswami, J., Howe, C.J., Huovelin, J., Koschny, D., Lawrence, D.J., Maddison, B.J., Maurice, S., Narendranath, S., Pieters, C., Okada, T., Rothery, D.A., Russell, S.S., Sreekumar, P., Swinyard, B., Wieczorek, M., Wilding, M., 2009. The scientific rationale for the C1XS X-ray spectrometer on India's Chandrayaan-1 Mission to the Moon. Planetary and Space Science, this volume, doi:10.1016/j.pss.2008.12.006.

Gow, J., Smith, D.R., Holland, A.D., Maddison, B., Howe, C., Sreekumar, P., Huovelin, J., Grande, M., 2007. In: Characterisation of swept-charge devices for the Chandrayaan-1 X-ray Spectrometer (C1XS) instrument-art. no. 66860I, OHW, UV, X-ray, and Gamma-ray Space Instrumentation for Astronomy XV 6686I6860-I6860.

Grande, M., 2001. The D-CIXS X-ray Spectrometer on ESA's SMART-1 mission to the Moon. Earth Moon and Planets 85–6, 143–152.

Grande, M., et al., 2003. The D-CIXS X-ray mapping spectrometer on SMART-1. Planetary and Space Science 51, 427–433.

Grande, M., et al., 2007. The D-CIXS X-ray spectrometer on the SMART-1 mission to the Moon—first results. Planetary and Space Science 55, 494.

Howe, C.J., Drummond, D., Edeson, R., Maddison, B., Parker, D.J., Parker, R., Shrivastava, A., Spencer, J., Kellett, B.J., Grande, M., Sreekumar, P., Huovelin, J., Smith, D.R., Gow, J., Narendranath, S., d'Uston, L., 2009. Chandrayaan-1 X-ray spectrometer (C1XS): instrument design & technical details. Planetary and Space Science, this volume, doi:10.1016/j.pss.2009.01.011.

Huovelin, J., Alha, L., Andersson, H., Andersson, T., Browning, R., Drummond, D., Foing, B., Grande, M., Hamalainen, K., Laukkanen, J., Lamsa, V., Muinonen, K., Murray, M., Nenonen, S., Salminen, A., Sipila, H., Taylor, I., Vilhu, O., Waltham, N., Lopez-Jorkama, M., 2002. The SMART-1 X-ray solar monitor (XSM): calibrations for D-CIXS and independent coronal science. Planetary and Space Science 50 (14–15), 1345–1353.

Jolliff, B.L., Gillis, J.J., Haskin, L.A., Korotev, R.L., Wieczorek, M.A., 2000. Major lunar crustal terranes: surface expressions and crust-mantle origins. Journal of Geophysical Resarch 105, 4197.

Joy, K.H., Crawford, I.A., Kellett, B., Grande, M.N., the C1XS Science Team, 2008. The Scientific Case for the Chandrayaan-1 X-ray Spectrometer. In: Lunar and Planetary Science XXXVIX, abstract no. 1070, 39th Lunar and Planetary Science Conference, Houston.

Keating, C.F., 2008. Not to worry: solar magnetic activity for cycle 24 is increasing. Eos Transactions 89 (43).

Kellett, B.J., et al., 2009. Planetary and Space Science, Manuscript, Submitted.

Lawrence, D.J., Feldman, W.C., Barraclough, B.L., Binder, A.B., Elphic, R.C., Maurice, S., Thomsen, D.R., 1998. Global elemental maps of the Moon: the Lunar prospector gamma-ray spectrometer 4 Sept 1998. Science 281.

Mewe, R., Gronenschild, E.H.B.M., van den Oord, G.H.J., 1985. Astronomy and Astrophysics Supplement 62, 197.

Racca, G.D., Marini, A., Stagnaro, L., van Dooren, J., di Napoli, L., Foing, B.H., Lumb, R., Volp, J., Brinkmann, J., Grunagel, R., Estublier, D., Tremolizzo, E., McKay, M., Camino, O., Schoemaekers, J., Hechler, M., Khan, M., Rathsman, P., Andersson, G., Anflo, K., Berge, S., Bodin, P., Edfors, A., Hussain, A., Kugelberg, J., Larsson, N., Ljung, B., Meijer, L., Mortsell, A., Nordeback, T., Persson, S., Sjoberg, F., 2002. SMART-1 mission description and development status. Planetary and Space Science 50 (14–15), 1323–1337.

Swinyard, B.M., Joy, K.H., Kellett, B.J., Crawford, I.A., Grande, M., Howe, C.J., Fernandes, V.A., Gasnault, O., Lawrence, D.J., Russell, S.S., Wieczoreki, M.A., Foing, B.H. The SMART-1 team. 2009. X-ray fluorescence observations of the moon by SMART-1/D-CIXS and the first detection of Ti Kα from the lunar surface. Planetary and Space Science, this volume, doi:10.1016/j.pss.2009.01.009.